Hybrid Deep Learning and First-Principles Model for Predictive Control of Solar Direct Steam Generation

Dibyajyoti Baidya[1], Ashutosh K Singh[2], Mani Bhushan[3] and Sharad Bhartiya[4]

***Abstract*— Linear Fresnel Reflector (LFR) systems for Direct Steam Generation (DSG) exhibit strong nonlinear and transient dynamics due to diurnal solar variability, making real-time control challenging. To address this, a Gated Recurrent Unit (GRU)-based deep neural network surrogate replaces the computationally intensive first-principles LFR model and is embedded within a Nonlinear Model Predictive Control (NMPC) framework for fast prediction. Trained using scheduled sampling, the surrogate achieves prediction fits of 87.39% for steam quality and 90.55% for LFR outlet pressure. The GRU-based LFR model is integrated with a first-principles Steam Drum (SD) model in a centralized NMPC scheme to regulate steam quality and drum water level. Closed-loop simulations under varying solar insolation with cloud cover demonstrate effective tracking of time-varying setpoints, validating the proposed hybrid predictive control approach.**

I. Introduction

Solar Thermal Power Plants (STPPs) convert solar radiation into high-temperature thermal energy for steam generation and power production. Their operation is strongly influenced by time-varying solar irradiance and ambient conditions, which directly affect heat input, steam formation, and overall plant performance [1], [2]. Achieving reliable operation under changing weather therefore requires models and control strategies capable of capturing nonlinear dynamics and maintaining key process variables within safe and efficient limits [3].

Among concentrated solar power technologies, the LFR has attracted significant research interest due to its compact layout, structural simplicity, cost effectiveness and suitability for DSG. A wide range of studies have addressed different modeling aspects of LFR systems. For instance, Ahmadpour et al. [4] developed a detailed optical model using Monte Carlo Ray Tracing to accurately capture solar ray reflections from curved primary mirrors and a dual-surface secondary reflector. Jessica et al. [5] proposed a nonlinear dynamic model based on the moving boundary formulation to describe two-phase flow and steam enthalpy evolution under operational constraints. Danish et al. [6] presented coupled nonlinear thermal and optical models for both conventional and greenhouse-enclosed LFR configurations, solving the governing equations numerically and employing ray-tracing analysis to evaluate optical losses and field efficiency. In parallel, Rowida et al. [7] investigated data-driven approaches, developing machine learning models trained on operational data to predict the output power of a Linear Fresnel plant. Despite these advances in optical, thermal, and performance modeling, dynamic models explicitly developed for control-oriented studies remain scarce. Existing dynamic representations are often either simplified through linearization or primarily intended for performance assessment rather than real-time operational control. Therefore, there is significant scope for developing a control-oriented data-driven model capable of accurately capturing system behavior over a wide range of operating conditions.

Industrial LFR plants typically employ decentralized control structures, which may overlook cross-coupling effects during transients [8], [9]. In a recent study, Kannaiyan et al. [8] has developed a detailed dynamic model of LFR, and later implemented decentralized PID control for LFR and SD subsystems [10]. Their work demonstrated that the plant has significant interaction and thus suitable for advance multivariate control strategy. As an advanced optimal control framework, Model Predictive Control (MPC) has gained significant prominence across various process industries due to its ability to handle multivariable interactions and operational constraints. However, applying conventional linear MPC to solar thermal systems remains challenging because of their inherently nonlinear, time-varying behavior, frequent startup and shutdown operations, and the presence of discrete operating modes [1]. These characteristics limit the effectiveness of linearized models and motivate the need for more suitable control-oriented modeling and nonlinear predictive control strategies.

The NMPC offers a suitable framework for handling multivariable interactions and constraints. However, implementing NMPC for integrated LFR–SD systems remains challenging due to dynamic model complexity and computational demands [11]. Thus, a gap remains in the implementation of real-time multivariable predictive control of integrated LFR–SD systems using models that are both accurate and computationally tractable. In recent literature, a data driven surrogate model of LFR-SD was employed for revenue optimization. while reducing the computational burden [2]. This suggests that a data driven nonlinear dynamic models can also be used in NMPC. In this work, the issue of computational complexity is addressed by replacing the high-fidelity LFR model with a gated recurrent unit (GRU)-based Deep Neural Network (DNN) surrogate model. The proposed model is trained using a dataset generated from the first-principles dynamic model, incorporating a scheduled sampling strategy during the training process. Further, the

[1]Dibyajyoti Baidya, [2]Ashutosh K Singh, [3]Mani Bhushan, [4]Sharad Bhartiya is with the Chemical Engineering Department, Indian Institute of Technology, Bombay, Maharashtra, 400076, India. [1]dibya_25@iitb.ac.in, [2]ashutosh23@iitb.ac.in, [3]mbhushan@iitb.ac.in, [4]bhartiya@che.iitb.ac.in

developed hybrid model is used as prediction model to implement NMPC which regulates steam quality and drum water level in LFR-SD.

The rest of the paper is organized as follows: Section II provides an overview and dynamic model of the LFR-SD. Section III discusses the data driven modeling of LFR and its validation. Section IV provides control objective and formulation of controller. Section V, discuss the controller performance and finally, Section VI presents the conclusion, highlighting future work and potential areas for further exploration.

II. Plant Overview and Dynamic Modeling

A. Plant Overview

In this study, attention is directed toward the LFR and SD assembly of a multi concentrator ([12]) STPP. Here, LFR and SD together form the DSG section of the plant [12]. The schematic Process Flow Diagram (PFD) of the LFR-SD is shown in Fig.1. The LFR field concentrates incident solar insolation onto a fixed receiver with the help of a mirror assembly. In the SD, feedwater is supplied from the deaerator and directed to the LFR absorber tubes, where it progressively undergoes phase change and forms a two-phase water–steam mixture. This two phase mixture then flows back to the SD, a crucial component that separates saturated steam from liquid water. The separated water is recirculated to the LFR, while the steam is delivered to the turbine assembly [8]. The LFR is rated at $2MW(th)$ with a total aperture area of $7020m^2$ and is designed for a DNI of $600W/m^2$. It consists of eight reflector rows, with U-shaped absorber tubes providing $480m$ flow length across eight parallel tubes. The system generates saturated steam at $44bar$ and $256°C$. The detailed design of the plant is already well described in the literature [13], [8].

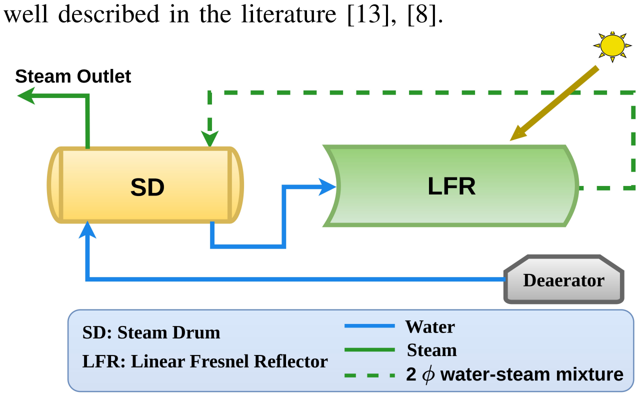

Fig. 1: PFD of LFR-SD

The LFR–SD system exhibits strongly nonlinear and non-stationary dynamic behavior. Specifically, diurnal solar insolation, together with cloud cover, acts as the primary disturbance, while startup, shutdown, and discrete operating conditions, further increase the operational complexity of the STPP. These factors result in highly nonlinear and time-varying plant dynamics, necessitating an accurate dynamic model to reliably capture and predict system behavior which will be discussed further.

B. LFR-SD first-principles dynamic model

1) LFR first-principles model: To represent the dynamic behavior of the system, the LFR is modeled using coupled one-dimensional partial differential equations (PDEs) describing the conservation of mass, momentum, and energy of the heat transfer fluid (HTF), along with energy balance equations for the absorber tube and glass envelope. The detailed dynamic model is already well described in literature [8]. These governing equations are discretized using the numerical scheme reported in the literature [8].

After spatial discretization using Chatoorgoon's method [14], these coupled PDEs are converted into 120,000 ordinary differential equations (ODEs) Owing to the very large number of ODEs, the LFR dynamic model is computationally intensive. A single-loop LFR simulation (10 hrs of operation) requires approximately 7.22 seconds [2], which makes its use in optimization and model-based control impractical. To address this limitation, a data-driven DNN based surrogate model of the LFR has been proposed, and discussed in the subsequent section.

2) SD first-principles model: The SD dynamics are described by an additional five ODEs that describe the dynamics of total mass in SD, mass of steam, mass of water, and with the steam and water enthalpies [8]. Which results in an overall LFR-SD model consisting of 120,005 ODEs [12]. The complete model structure and variable definitions are available in the referenced literature [8]. Note that only the governing daytime equations relevant to the this work are summarized below [8], [12]:

$$\frac{dM_{(w,SD)}}{dt} = \dot{m}_{(w,i,SD)} - \dot{m}_{(w,o,SD)} + \dot{m}_{(w,fresh)} \tag{1}$$

$$\frac{dM_{(st,SD)}}{dt} = \dot{m}_{(st,i,SD)} - \dot{m}_{(st,o,SD)} \tag{2}$$

$$\begin{aligned}\frac{dh_{(w,SD)}}{dt} = \frac{1}{M_{(w,SD)}}\Big(&\dot{m}_{(w,i,SD)}h_{(w,i,SD)} - \dot{m}_{(w,o,SD)}h_{(w,SD)} \\ &+ \dot{m}_{(w,fresh)}h_{(w,fresh)} - h_{(w,SD)}\frac{dM_{(w,SD)}}{dt}\Big)\end{aligned} \tag{3}$$

$$\begin{aligned}\frac{dh_{(st,SD)}}{dt} = \frac{1}{\rho_{(st,SD)}\left(V_{SD} - \frac{M_{(w,SD)}}{\rho_{(w,SD)}}\right)}\Big(&\dot{m}_{(st,i,SD)}h_{(st,i,SD)} \\ &- \dot{m}_{(st,o,SD)}h_{(st,SD)} - h_{(st,SD)}\frac{dM_{(st,SD)}}{dt}\Big)\end{aligned} \tag{4}$$

$$P_{SD} = f\left(h_{(st,SD)}, \rho_{(st,SD)}\right) \tag{5}$$

$$\dot{m}_{(st,o,SD)} = K_v\sqrt{\max(P_{SD} - P_{SG},\, 0)} \tag{6}$$

In [8], the detailed first-principles model is validated component wise with the real plant data along with the plant operation procedure and simulation approach [12], [15].

III. Data Driven Modeling of LFR and Validation

To develop a control-relevant model of the LFR, a gated recurrent unit (GRU)-based DNN has been developed to predict steam quality and the LFR outlet pressure. The LFR outlet pressure represents a key state that directly influences the SD dynamics, along with steam quality which serve as the controlled variable.

To replace the first-principles LFR model with a GRU-DNN surrogate, a total of 69,000 time-series data points are generated using the integrated LFR–SD first-principles model, as illustrated in Fig. 2. The dataset corresponds

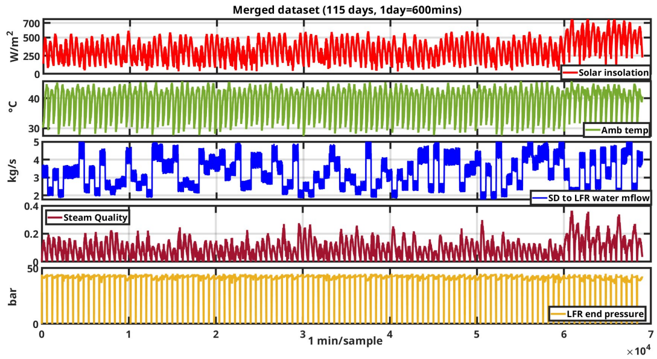

Fig. 2: DNN training input-output dataset

to 115 simulated days, with each day representing 600 minutes sampled at 1 minute. The solar insolation profile for each day is designed to realistically mimic diurnal patterns, including sunrise, peak intensity, sunset, and varying cloud cover conditions. Consequently, a wide range of weather scenarios, such as sunny, cloudy, and partly cloudy days are captured. To generate data for the DNN training, the water mass flow rate from the SD to the LFR ($\dot{m}$) along with the two disturbances namely solar insolation (I) and ambient temperature (T_{amb}) is perturbed within its nominal operating range. Using these perturbed inputs, simulation data are generated for steam quality at the end of the LFR pipe and LFR outlet pressure. Using this simulated dataset GRU based DNN (GRU-DNN) surrogate model for the LFR is developed and discussed in the subsequent section.

A. *Surrogate modeling framework for LFR*

A GRU-DNN surrogate sequential architecture has been developed to predict the steam quality and the LFR outlet pressure, as illustrated in Fig. 3, which replaces the first prinicples LFR (Fig. 1). Separate network structures are designed for each output for better model accuracy. The steam quality model (GRU-DNN-1) uses two GRU layers with 128 and 48 neurons, while the LFR outlet pressure model (GRU-DNN-2) uses two GRU layers with 128 and 64 neurons which is shown in Fig. 3.

1) LFR Steam Quality Prediction (GRU-DNN-1): The input vector to the GRU-DNN-1 model is constructed as shown in Equation 7. Here, k denotes the current time instant. The terms $k-1$, $k-2$, and $k-3$ represent the first, second, and third previous time delay respectively for better model accuracy. The number of lags in the input features is selected based on a systematic trial-and-error procedure to achieve optimal predictive performance. In this work, for simplicity, the notation $\dot{m}_{(w,o,SD)}$ is hereafter represented as $\dot{m}_w$.

$$\begin{aligned}\mathbf{X}_Q(k) = \Big[&\dot{m}_w(k),\ \dot{m}_w(k-1),\ \dot{m}_w(k-2),\ \dot{m}_w(k-3),\ I(k),\\ &I(k-1), I(k-2),\ I(k-3),\ T_{\text{amb}}(k),\ T_{\text{amb}}(k-1),\\ &T_{\text{amb}}(k-2),\ T_{\text{amb}}(k-3),\ Q(k)\Big]^T\end{aligned} \tag{7}$$

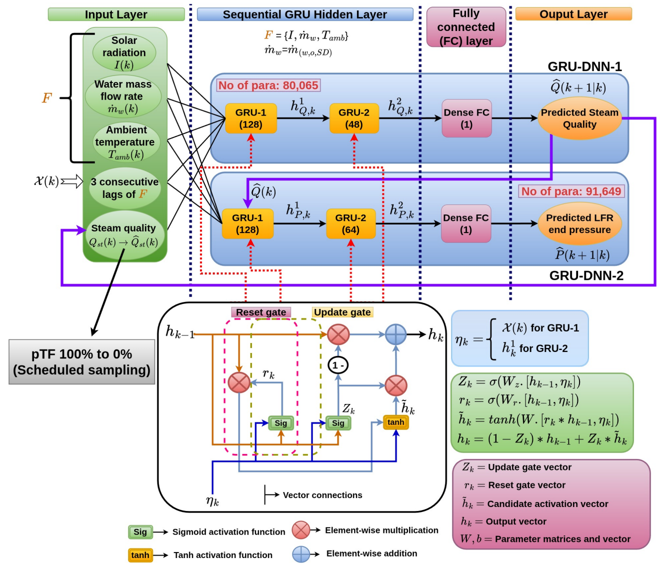

Fig. 3: GRU surrogate architecture of LFR

Note that the steam quality ($Q(k)$) is included as one of the input features to capture the system's autoregressive dynamics. During training, the true past output is fed back to the network as an input following the classical teacher forcing (TF) strategy [2], enabling the model to learn the recursive dependency of the current prediction on its previous values. However, during testing or deployment, the true steam quality is not available, therefore, the network must rely on its own previous predictions as inputs for future time steps. This mismatch between training and inference can lead to error accumulation over long horizons, potentially resulting in drift or instability during closed-loop operation.

To mitigate this issue, scheduled sampling is incorporated into the training process [16]. Scheduled sampling gradually exposes the network to its own predictions during training, thereby reducing the mismatch between training and deployment. At each time step, the steam quality ($Q(k)$) is selected probabilistically as input feature shown below:

$$Q(k) = \begin{cases} Q_{st}(k), & \text{with probability } p_{\text{TF}} \\ \widehat{Q}_{st}(k), & \text{with probability } 1 - p_{\text{TF}} \end{cases} \tag{8}$$

where $p_{\text{TF}} \in [0,1]$ denotes the teacher-forcing probability, Q_{st} is true and $\widehat{Q}_{st}$ is the predicted steam quality respectively.

The value of p_{TF} is gradually decreased as the number of training epochs increases. During the initial training stages, the model relies mainly on true historical outputs to ensure stable learning. As training progresses, predicted outputs are increasingly fed back as inputs, enabling the network to learn to operate under closed-loop conditions. This approach does not modify the network architecture. Instead, it changes the training regime. Initially, learning resembles a nonlinear autoregressive with exogenous input (NARX) formulation, where true past outputs are available. As scheduled sampling reduces reliance on ground-truth outputs, the learning scenario moves closer to a nonlinear output error (NOE) formulation, where the model must depend on its own predictions. This transition improves robustness to error accumulation and enhances long-horizon predictive performance during deployment. The GRU learns the nonlinear mapping of steam quality as shown in the equation below:

$$\widehat{Q}(k+1) = f_{GRU_1}\Big(\mathbf{X}_Q(k), \mathbf{h}_\mathbf{Q}(k), \theta_Q\Big); \quad \theta_Q \in [W, b] \tag{9}$$

where, $\mathbf{h}(k)$ is the hidden state output of the GRU and θ_Q represents the network parameters (refer to Fig. 3).

2) LFR outlet pressure prediction (GRU-DNN-2): The input vector to the GRU-DNN-2 model is constructed as shown in Equation 10, where the predicted output ($\widehat{Q}(k)$) of GRU-DNN-1 is also used as input feature while training.

$$\begin{aligned}\mathbf{X}_P(k) = \Big[&\dot{m}_w(k),\, \dot{m}_w(k-1),\, \dot{m}_w(k-2),\, \dot{m}_w(k-3),\\ &I(k),\, I(k-1), I(k-2),\, I(k-3), T_{amb}(k),\\ &T_{amb}(k-1),\, T_{amb}(k-2),\, T_{amb}(k-3), \widehat{Q}(k)\Big]^T\end{aligned} \tag{10}$$

The network mapping for the LFR end pressure is given by the following equation:

$$\widehat{P}(k+1) = f_{GRU_2}\Big(\mathbf{X}_P(k), \mathbf{h}_\mathbf{P}(k), \theta_P\Big); \quad \theta_P \in [W, b] \tag{11}$$

3) Validation of the LFR GRU model: The proposed GRU-DNN surrogate models are validated under long-horizon rollout conditions (recurrent mode) over time horizon of 600 minutes. During testing, the models are simulated using input dataset of solar insolation, mass flow rate of water from SD to LFR and ambient temperature along with their predicted lagged values, thereby emulating real-time deployment. A multistep validation scenario is considered in which the water mass flow rate from the SD to the LFR is deliberately perturbed, as illustrated in Fig. 4. The same input trajectories are simultaneously applied to both the first-principles LFR–SD model (discussed in Section II-B) and the GRU-DNN surrogate models to enable performance comparison.

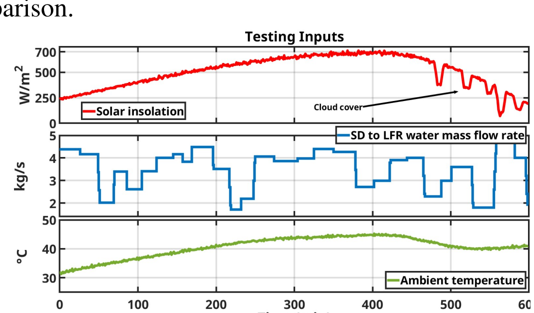

Fig. 4: Testing dataset for LFR GRU-DNN

The prediction results, shown in Fig. 5, demonstrate stable and accurate long-horizon simulation along with the LFR GRU surrogate model achieving a computational time of only 0.000729 sec for a 10-hour operation run which is more then 9000 fold faster then first-principles based LFR model. Based on the normalized root mean squared error (NRMSE), the obtained percentage fit values are 87.39% for steam quality

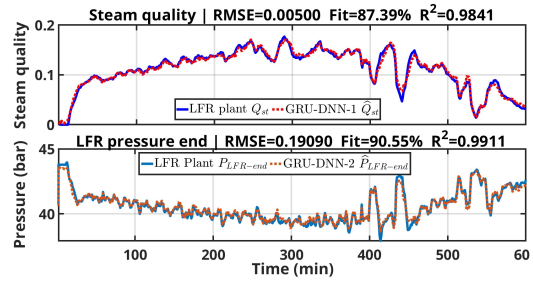

Fig. 5: Model comparison of LFR GRU-DNN and LFR plant

and 90.55% for LFR end pressure. The corresponding RMSE values are 0.00500 and 0.19090, while the coefficients of determination R^2 are 0.9841 and 0.9911, respectively (see Fig. 5). It has been observed that no drift is observed during the closed-loop rollout, indicating the learned dynamics of the GRU-DNN surrogate model preserve the inherent dynamic characteristics of the physical system. This confirms the suitability of the proposed GRU-DNN surrogate models for integration into predictive control frameworks which requires reliable multistep ahead prediction. The developed GRU-DNN surrogate model for the LFR, together with the first-principles model of the SD, is employed as the prediction model within the NMPC framework, which is discussed in the following section.

IV. CONTROL OBJECTIVE OF LFR-SD AND CONTROLLER FORMULATION

In this section, NMPC is implemented to control the key variables at the desired setpoint. Fig. 6 shows the proposed NMPC control architecture.

For the control study, the controlled variables (CVs), manipulated variables (MVs), and disturbance variables (DVs) have been chosen and are summarized in Table I.

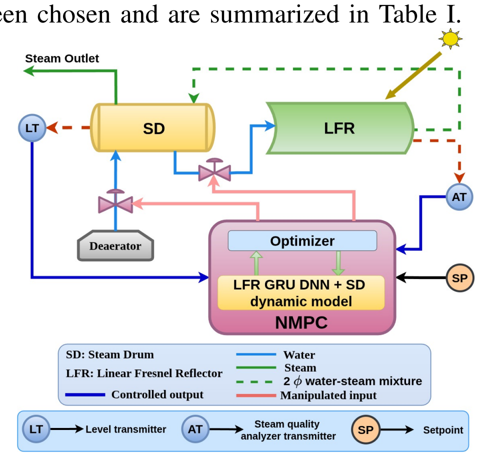

Fig. 6: Block diagram of NMPC Control architecture

TABLE I: Summary of CV, MV and DV for LFR-SD

	LFR	SD
CV	Steam quality (Q_{st})	Water level in SD ($H_{w,SD}$)
MV	Water mass flow rate from SD to LFR ($\dot{m}_w$)	Fresh water mass flow rate to SD from Deaerator ($\dot{m}_{w,fresh}$)
DV	Solar radiation (I), Ambient temperature (T_{amb})	Mass flow rate of steam out from the SD ($\dot{m}_{st,o,SD}$)

A. Design of setpoint

The setpoints for steam quality and drum level are derived from a plant-wide revenue optimization study reported in the literature [2]. The plantwide revenue optimization was carried out in presence of the solar radiation and ambient temperature profile as shown in Fig. 7 (Solar insolation profile case-1: SI-1, Ambient temperature profile case-1: T_{Amb}-1). This particular revenue optimization accounts for variations in market electricity demand. The optimization framework determines an optimal mass flow rate profile of SD to LFR that maximizes electricity production. This optimal profile is applied to the LFR–SD system in open-loop simulation to generate the corresponding steam quality and drum level trajectories. These trajectories represent the nominal operating conditions associated with the revenue-optimized scenario and are therefore adopted as the control setpoints in the present work.

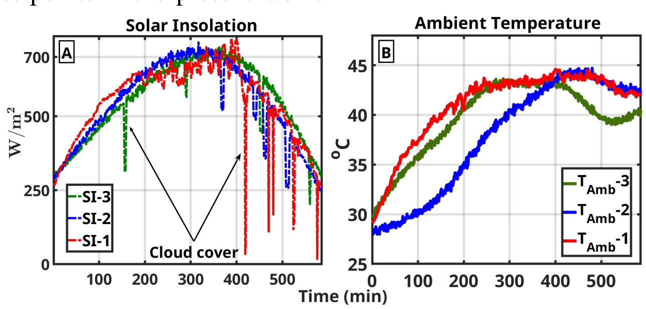

Fig. 7: [A] Solar insolation profiles, [B] Ambient temperature profiles (Solar insolation (SI)-case)

B. Control Objective

The control objectives for LFR-SD are defined as follows:

1) The steam quality at the LFR outlet (Q_{st}) is required to track the time-varying setpoint obtained from the plant-wide revenue optimization framework [2].
2) The level of liquid in the SD ($H_{w,SD}$) should also track the water level setpoint necessary to maintain the quality of the steam at the LFR outlet. Note that the height of water in SD is determined by converting the liquid volume into level using the analytical volume–height relation for a horizontal cylinder [10].

Note that, the tracking must be achieved in the presence of measured external disturbances namely solar radiation and ambient temperature, illustrated as SI-3 and T_{Amb}-3 in Fig. 7A and Fig. 7B, respectively. Although the exact future values of these disturbances are unknown, their forecasted disturbance profiles are assumed to be available (forecasted) for controller implementation. The forecasted solar radiation and ambient temperature are used as the nominal disturbances in NMPC and are shown in Fig. 7 as SI-2 and T_{Amb}-2, respectively.

C. NMPC formulation

In this work, the NMPC formulation is adopted from Baidya et al. [1]. To simplify notation, we define a few set of variables. The measurement ($Y(k)$), control input ($U(k)$), measured disturbance ($D(k)$) as shown in SI-3 and T_{Amb}-3 of Fig. 7, forecasted disturbance profile ($\widetilde{D}$) as shown in SI-2 and T_{Amb}-2 of Fig. 7, and setpoint ($R(k)$) at k^{th} time instant is defined as follows:

$$Y(k) \triangleq [Q_{st} \quad H_{w,SD}]^T, \quad U(k) \triangleq [\dot{m}_w \quad \dot{m}_{(w,fresh)}]^T$$
$$D(k) \triangleq [I \quad T_{amb}]^T, \ \widetilde{D} \triangleq [\widetilde{I} \quad \widetilde{T}_{amb}]^T, \ R(k) \triangleq [Q_{\text{sp}} \ H_{\text{sp}}]^T$$

where, I is measured solar insolation at k^{th} instant, and $\widetilde{I}$ denotes the forecasted solar insolation profile. Similarly, T_{amb} is measured ambient temperature at k^{th} instant and $\widetilde{T}_{amb}$ denotes the forecasted ambient temperature profile. The variables Q_{sp} and H_{sp} represent the setpoints (R) for the LFR outlet steam quality and the liquid level in the SD.

At every sampling instant k, given the measurement ($Y(k)$) and forecasted disturbances profile ($\widetilde{D}$), the NMPC cost function is given as follows:

$$J(k) = \sum_{i=1}^{N_p} \left\| E(k+i|k) \right\|^2_{W_E} + \sum_{i=0}^{N_c-1} \left\| \Delta U(k+i|k) \right\|^2_{W_{\Delta U}} \tag{12}$$

where,

$$E(k+i|k) = \widehat{Y}(k+i|k) - R(k) + \widehat{e}_f(k)$$
$$\Delta U(k+i|k) = U(k+i|k) - U(k+i-1|k)$$

The notation $\|(.)\|_W$ denotes the weighted norm, where $W \succ 0$. N_p and N_c are the prediction and control horizons respectively. Note that, in this NMPC formulation, predicted output correction is done by adding constant filtered innovation $\widehat{e}_f(k)$ which is defined as follows:

$$\widehat{e}_f(k) = \alpha \widehat{e}_f(k-1) + (1-\alpha) e(k), \text{and}$$
$$e(k) = Y(k) - \tilde{f}_{comb}\left(\widehat{Y}(k), U(k),\ D(k)\right) \tag{13}$$

Here, α represents tuning parameter such that $0 < \alpha < 1$.

Now, the optimization problem to be solved at every sampling instant k is given as:

$$\min_{U(k+i|k),\ i=0,1\ldots N_p-1} J(k)$$

subjected to,

$$\widehat{Y}(k+i|k) = \tilde{f}_{comb}\left(\widehat{Y}(k+i-1|k), U(k+i-1|k), \mathcal{D}(k+i-1)\right)$$
$$U_{\min} \le U(k+i|k) \le U_{\max}, \quad i = 0, \ldots, N_c - 1,$$
$$\Delta U_{\min} \le \Delta U(k+i|k) \le \Delta U_{\max}, \quad i = 0, \ldots, N_c - 1,$$
$$U(k+i|k) = U(k+N_c-1|k), \quad i = N_c, \ldots, N_p - 1$$

Here, $\tilde{f}_{comb}$ is the combination of GRU-DNN surrogate of LFR (Eqns. 9 & 11) and SD first-principles model (Eqns. 1 to 6). Furthermore, at k^{th} instant, the difference of measured disturbance $D(k)$ and the forecasted disturbance $\widetilde{D}(k)$ is used as the bias correction of disturbance in the prediction model as follows:

$$\mathcal{D}(k+i-1) = \widetilde{D}(k+i-1) + \Delta D(k),\ i = 1, 2..N_p$$
$$\Delta D(k) = D(k) - \widetilde{D}(k) \tag{14}$$

After solving above optimization problem, the optimal control input trajectory, $U(k+i|k)$ for $i = 0, 1, \ldots, N_p$ is obtained. But, only the first move $U(k|k)$ is applied to the process and at the next sampling instant the optimization problem is solved again within a receding horizon framework.

V. CLOSE-LOOP PERFORMANCE ANALYSIS OF THE NMPC FOR LFR-SD

In this section, we present the performance analysis of the formulated NMPC scheme described in Section IV for regulating the steam quality at the LFR outlet and the liquid level in the SD. For the performance analysis of NMPC, the Mean Squared Error (MSE) is calculated, which is defined as follows:

$$\mathrm{MSE} = \frac{1}{N_s} \sum_{k=1}^{N_s} \left\| Y(k) - R(k) \right\|_{W_E}^2 \tag{15}$$

Here, N_s is the total number of samples considered in the simulation study. The tuning parameters of NMPC chosen in this control study are: $N_P = 15$, $N_C = 5$, $W_E = diag[100 \quad 70]$, $W_{\Delta U} = diag[0.2 \quad 0.2]$, $\alpha = 0.9$, $U_{min} = [1.4 \quad 10^{-5}]$, $U_{max} = [5 \quad 0.8]$, $\Delta U_{min} = [-1 \quad -0.8]$, $\Delta U_{max} = [1 \quad 0.8]$.

Fig. 8 and Fig. 9 show the NMPC closed-loop performance along with openloop. It is evident from Fig. 8, that the NMPC controller is able to track the time varying setpoints of LFR steam quality and SD water level. The open-loop simulation is carried out using the optimal mass flow rate profile (Fig. 9), which is also used to generate the corresponding setpoint trajectory. The disturbance input $D(k)$ (see SI-3, T_{Amb}-3) is applied as shown in Fig. 7. The results show that the system is unable to maintain the desired setpoint under disturbance conditions in open loop, thereby necessitating the implementation of an NMPC framework for effective setpoint tracking. The MSE is 0.155 in openloop and 0.084 with NMPC, corresponding to approximately a 45.8% reduction in tracking error. Fig. 9 shows the NMPC manipulated inputs behaviour.

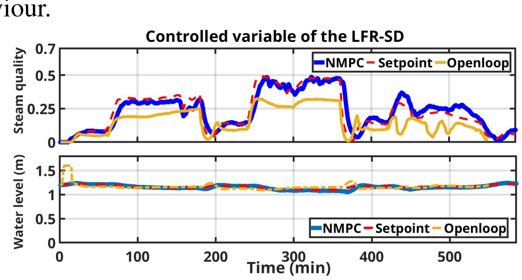

Fig. 8: NMPC CV comparison of OC-1 and OC-2

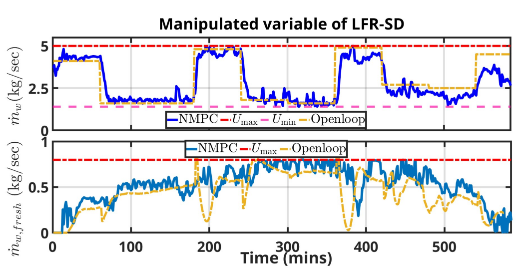

Fig. 9: NMPC MV comparison of OC-1 and OC-2

VI. CONCLUSION

In this work, a hybrid modeling and control framework for LFR–SD systems is developed to enable real-time predictive control under dynamic conditions. Replacing the first-principles LFR model with a GRU-based surrogate significantly reduces computational burden, making nonlinear model predictive control feasible for online implementation. The use of scheduled sampling during training improves the robustness of multi-step predictions, which is critical for closed-loop control applications. By integrating the data-driven LFR model with a physics-based SD model, the proposed NMPC scheme effectively regulates both steam quality and drum water level under time-varying operating conditions and solar disturbances.

REFERENCES

[1] D. Baidya, S. Kannaiyan, and N. D. Bokde, "Study of parabolic trough collector with crucial analysis on controller and estimator with variable mirror efficiency," Journal of Process Control, vol. 143, p. 103317, 2024.

[2] D. Baidya, S. Kannaiyan, M. Bhushan, and S. Bhartiya, "Plantwide dynamic optimization of a hybrid solar thermal power plant using deep neural network modeling," SSRN Electronic Journal, 2025.

[3] P. Velarde, A. J. Gallego, C. Bordons, and E. F. Camacho, "Scenario-based model predictive control for energy scheduling in a parabolic trough concentrating solar plant with thermal storage," Renewable Energy, vol. 206, pp. 1228–1238, 2023.

[4] A. Ahmadpour, A. Dejamkhooy, and H. Shayeghi, "Optimization and modelling of linear fresnel reflector solar concentrator using various methods based on monte carlo ray–trace," Solar Energy, vol. 245, pp. 67–79, 2022.

[5] J. Leo, C. Kharrat, A. Voda, G. Besancon, and F. Davelaar, "Modeling and control of a Linear Fresnel Reflector for an Integrated Solar Combined Cycle," in ECC 2014 - 13th European Control Conference, Strasbourg, France, Jun. 2014, p. n/c.

[6] S. N. Danish, Z. Almutairi, A. El-Leathy, H. Al-Ansary, Y. Jardan, and S. Alaqel, "Modeling and performance simulation of an innovative concept of linear fresnel reflector based csp system," Journal of Thermal Science, vol. 30, no. 5, pp. 1614–1624, 2021. [Online]. Available: https://doi.org/10.1007/s11630-021-1457-9

[7] R. Meligy, A. Montenon, and H. A. Hassan, "Comparative analysis of machine learning models of linear fresnel solar collector," Renewable Energy, vol. 230, p. 120865, 2024.

[8] S. Kannaiyan, S. Bhartiya, and M. Bhushan, "Dynamic modeling and simulation of a hybrid solar thermal power plant," Industrial & Engineering Chemistry Research, vol. 58, no. 18, pp. 7531–7550, 2019.

[9] L. Bodini, L. Delale, J.-L. Nouet, and B. Dumercq, "Control laws for a linear fresnel reflector solar steam generator in once-through mode on a commercial operating power plant," Journal of Solar Energy Engineering, vol. 141, no. 3, p. 031012, 11 2018.

[10] S. Kannaiyan, S. Bhartiya, and M. Bhushan, "Plantwide decentralized controller design for hybrid solar thermal power plant," Frontiers in Control Engineering, vol. 3, 2022.

[11] D. Baidya, M. Bhushan, and S. Bhartiya, "Revenue optimization for dynamic operation of a hybrid solar thermal power plant," in Proceedings of the 35th European Symposium on Computer Aided Process Engineering (ESCAPE-35), 07 2025, pp. 1101–1107.

[12] D. Baidya, S. Kannaiyan, M. Bhushan, and S. Bhartiya, "Plantwide dynamic simulation of hybrid solar thermal power plant with molten salt thermal energy storage," Renewable Energy, vol. 255, p. 123794, 2025.

[13] J. Nayak, S. Kedare, R. Banerjee, S. Bandyopadhyay, N. Desai, S. Paul, and A. Kapila, "A 1 MW national solar thermal research cum demonstration facility at Galpahari, Haryana, India," Current Science, pp. 1445–1457, 2015.

[14] V. Chatoorgoon, "Sports-a simple non-linear thermalhydraulic stability code," Nuclear Engineering and Design, 1986.

[15] D. Baidya, S. Kannaiyan, M. Bhushan, and S. Bhartiya, "Hysolsim: A digital twin (simulator) for hybrid solar thermal power plant," SSRN Electronic Journal, 2025.

[16] S. Bengio, O. Vinyals, N. Jaitly, and N. Shazeer, "Scheduled sampling for sequence prediction with recurrent neural networks," in Advances in Neural Information Processing Systems, C. Cortes, N. Lawrence, D. Lee, M. Sugiyama, and R. Garnett, Eds., vol. 28. Curran Associates, Inc., 2015.